Journal of Materials Chemistry A

ROYAL SOCIETY OF CHEMISTRY

COMMUNICATION

View Article Online
View Journal | View Issue

Cite this: J. Mater. Chem. A, 2024, 12, 31116

Received 15th August 2024
Accepted 28th October 2024

DOI: 10.1039/d4ta05747c

rsc.li/materials-a

A new approach for obtaining ceramic NASICON ($Na_3Zr_2Si_2PO_{12}$) films sintered *in situ* by a sol–gel method, using spray deposition and near-infra red sintering†

Rafael Marti Valls, ‡[a] Rebecca Griffin,‡[ab] Anne Sawhney, [a] Celina Domingos-Dlofo,[a] Tom Dunlop, [a] Sam Reis,[a] Peter J. Holliman [a] and Jenny Baker *[ab]

In this work we demonstrate a NASICON film sintered *in situ* onto a fused silica substrate. This production method drastically reduces the manufacturing time by combining the use of a spray-coated sol–gel solution and near-infrared (NIR) ultrafast sintering technology. This is the first demonstration of NIR sintered ceramics at high temperatures (~1000 °C).

Sodium super ionic conductors (NASICONs) have been widely studied thanks to their unique properties for applications such as harmful gas sensing (*e.g.* NO_x, CO_2, SO_2 or H_2S),[1,2] ion selective membranes[3,4] or as solid electrolytes in sodium-ion batteries (SIBs).[5–7] Depending on the application, modifications on the structure have been tested to increase conductivity or reduce detrimental secondary phases, among others.[7–9] Several synthetic routes have been studied to produce NASICON structures[10] where solid-state,[5,6,11,12] co-precipitation[13–15] and sol–gel[1,13,16–20] methods stand out. Solid state methods present a lower chemical preparation complexity than the co-precipitation and sol–gel methods. However, the processing, multiple ball milling and pressing steps where yield loss at each step can be significant, combined with multiple sintering steps significantly increase production time for solid-state (SS) produced NASICON discs/pellets. Thin (86 micron thick) stand-alone films (precursor powder prepared through the SS method) have been demonstrated in batteries with a capacity of 73 mA h g^{-1},[21] but replicating thin stand-alone ceramic electrolytes on large area batteries will prove difficult due to the fragility of the stand-alone film.

By comparison, the sol–gel method requires a more sophisticated processing route to obtain the appropriate chemical precursors, the application of different temperatures during the production process, a specific order of addition for the chemicals or the control of their addition rate.[22] This extra care in the manufacture of precursors yields more homogeneous materials and leads to shorter sintering times (~15 hours compared with >40 hours), which results in the method being more sustainable in terms of energy consumption.[23] The sol preparation process can also be simplified by using water instead of an organic solvent, *e.g.*, ethanol.[22] Shimizu *et al.* designed a water-based sol–gel method to obtain high-purity $Na_3Zr_2Si_2PO_{12}$ powders by mixing the inorganic precursors dissolved in a certain order.[17] They also developed a method to prepare NASICON films directly from the precursor mixture by modifying the previously mentioned aqueous solution with an hydroxyacid to increase the solution viscosity and stability and subsequently depositing it by spin-coating.[18] The films required 15 hours (5 × 3 hours) of sintering in a conventional electric furnace at 1000 °C and produced NASICON films on alumina with some zirconia impurities. This method allows obtaining a sol that is sufficiently stable. A modification of this method was used in this work. Specifically, we fabricated NASICON films by spray deposition instead of spin coating. Spray deposition of other ceramic materials has been shown to substantially simplify the production process, facilitate scalability and enhance controllability.[24]

Another limiting step in the NASICON production is the long times of sintering at high temperature typically using radiant heat ovens which can cause secondary phases such as zirconia.[18] Non-conventional techniques have been used to greatly reduce the sintering time of NASICONs, such as, ultra-fast high temperature sintering,[25] spark plasma sintering[26] and microwave sintering.[27] Whilst these techniques allow for very fast sintering, they also have some disadvantages, such as (1) the ultra-fast high temperature sintering technique requires the use of an inert argon atmosphere to protect the carbon tooling connectors; (2) the spark plasma technique can only sinter a small area at a time; and (3) the microwave technique is a batch process. An alternative to vastly decrease sintering times

[a]Swansea University Bay Campus, Fabian Way, Swansea, UK

[b]Faculty of Engineering and Design, University of Bath, BA2 7AY, UK. E-mail: jb4251@bath.ac.uk

† Electronic supplementary information (ESI) available: S1-thermal stage XRD results, S2-video of the NIR sintering process, S3-plan view of the NASICON film on fused silica disc Pt-sputtered and Ag-coated (ionic resistivity measurement) characterisation equipment. See DOI: https://doi.org/10.1039/d4ta05747c

‡ These authors contributed equally to the preparation of this manuscript.

and potentially avoid the drawbacks of the previously mentioned techniques is heating with near infrared (NIR) radiation. This technology was studied in the present work. NIR heating differs from traditional IR heating in that the lamps emit at a much higher energy density (up to 5 times higher),[28] and is based on the absorption of infrared radiation (900–1200 nm) emitted by an element present in the sample (*e.g.*, the substrate).[29] Electromagnetic radiation is rapidly absorbed allowing a much faster sintering than conventional furnaces which transfer heat to the sample more slowly by a mixture of radiation, convection and conduction.[30] Whilst NIR has been used to fast sinter metals[31,32] and metal oxides,[33–36] to the best of the authors' knowledge, the highest sintering temperature demonstrated using in-line NIR processing prior to this work is 450 °C.[37]

A precursor NASICON sol was produced by dissolving ammonium dihydrogen phosphate ($NH_4H_2PO_4$, 0.17 g, 1.5 mmol, Fisher Scientific) in H_2O (7.34 g) and sodium metasilicate nonahydrate ($Na_2SiO_3 \cdot 9H_2O$, 0.85 g, 3 mmol, Sigma Aldrich) in H_2O (10.00 g). The $NH_4H_2PO_4$ solution is then added to the $Na_2SiO_3 \cdot 9H_2O$ solution and stirred. Tartaric acid ($C_4H_6O_6$, 0.67 g, 4.5 mmol, Fisher Scientific) was then added and stirred until dissolved. Zirconyl chloride ($ZrOCl_2 \cdot 8H_2O$, 0.97 g, 3 mmol, Fisher Scientific) was then dissolved in H_2O (30.00 g) and stirred >48 h before filtering through a 0.45 μm PTFE syringe filter (Fisher Scientific). The zirconyl chloride solution was added dropwise to the original sample and stirred for 1 h. A 5% solid solution was obtained with a molar ratio of 4 : 2 : 2 : 1 (Na : Zr : Si : P, sodium excess improves $Na_3Zr_2Si_2PO_{12}$ formation[20]). To produce a powder the sol was dried, calcined and sintered at 1000 °C as detailed by Shimizu,[18] producing NASICON powder with negligible secondary phases (Fig. 1a). The differential thermal analysis of the dried sol–gel solution (dried at 120 °C, Fig. 1b) shows that at the sintering temperature applied, undesired molecules are absent, *e.g.*, physically adsorbed water[38] (dTG peak at 88 °C associated with an endothermic reaction, number 1 in Fig. 1b), ammonia from $NH_4H_2PO_4$ (ref. 38) and unbounded tartaric acid[39] (dTG peak at 255 °C, associated with an endothermic reaction, number 2 in Fig. 1b) and organic molecules coordinated to Zr^{4+} ref. 39 (dTG peaks at 366 °C and 977 °C, both related to exothermic carbon combustion reactions, numbers 3 and 4 in Fig. 1b, respectively). The data also show peaks related to the melting of NaCl around 800 °C and a loss of mass at higher temperatures (number 5 in Fig. 1b, dTG at 1055 °C associated with an endothermic peak). It could be related to the evaporation of sodium chloride.[17] The loss of sodium would explain the presence of small secondary phases in the sintered powder (Fig. 1a).

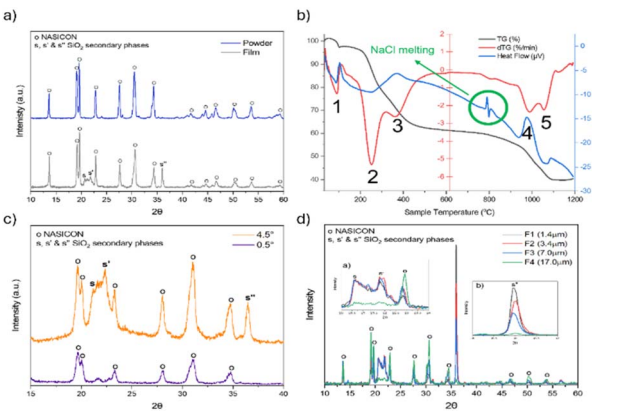

Fig. 1 (a) XRD of NASCION powder and the NASICON film on fused silica, (b) DSC-TGA analysis of dried sol, (c) GI-XRD of the NASICON film at 0.5° and 4.5°, and (d) XRD of NASICON films with different film thicknesses on fused silica substrate.

To create a thin film, a spray process was developed based on a method used to create compact TiO_2 films[40] which is suitable for large area manufacturing. This involved using an artist spray gun (Amazon) to spray the sol, at a nitrogen pressure of 4 bar, onto a fused silica substrate heated to 120 °C (high temperature titanium hot plate), depositing multiple layers to build up the desired thickness. The substrate was pretreated by plasma irradiation (O_2 plasma cleaner) for 15 min to improve surface wettability. Once the sample was dried, it was sintered at 1000 °C in air for 3 h. XRD of the resulting film (Fig. 1a) shows that the film mainly consists of a NASICON with some low intensity SiO_2 secondary phases (s for tridymite, orthorhombic silica, COD 9013393, and s′ and s″ for cristobalite, tetragonal silica, COD 9001578). Grazing incidence XRD (GI-XRD, Fig. 1c) demonstrates that these silica phases were not present on the top surface of the film and are likely the result of the formation of a crystalline silica phase at/near the surface of the substrate. This is confirmed in Fig. 1d by the reduction in the intensity of the peaks of these phases with increasing film thickness.

To reduce the sintering time of the NASICON film from hours to 60 s, near-infrared sintering was employed. By using lamps (adphosNIR® 6 × 6 kW) with the same energy density profile as those used in previous work (peak wavelength intensity of 900–1200 nm,[37] Fig. 2a) but reducing the sample-to-lamp distance, the view factor of the systems was increased, leading to a rise in the energy absorbed by the sample. Further design improvements of the system, such as active cooling of the electronics and the implementation of a ceramic transport system with a quartz bed, permitted temperatures >1000 °C to be reached.

Both fused silica and the dried sol absorb NIR wavelengths poorly (number 1 and 2, Fig. 2b) and therefore direct NIR heating of sprayed sol (NIR oven power at 90% for 60 s, 30 layers sprayed) does not result in a temperature high enough to form a NASICON (diffractogram A, Fig. 2c). It only formed tetragonal (z′ and z‴, COD 1526427) and monoclinic (z and z″, COD 2300544) zirconium oxide phases. The crystallisation of these zirconium phases suggests that absorption of longer wavelength IR radiation (>2000 nm) happened, *e.g.*, by Si–O and P═O bonds (bonds present in the sample and well-known absorbers of far-infrared radiation). However, the number of photons emitted by the lamps in this region of the spectrum is not enough to reach the fast formation of the NASICON phase.

The tartaric acid contained in the film generates a black carbon-rich intermediate after 1 h of heat treatment at 750 °C in air. This material acts as a susceptor that absorbs strongly between 600 and 2000 nm (number 5, Fig. 2b), and therefore

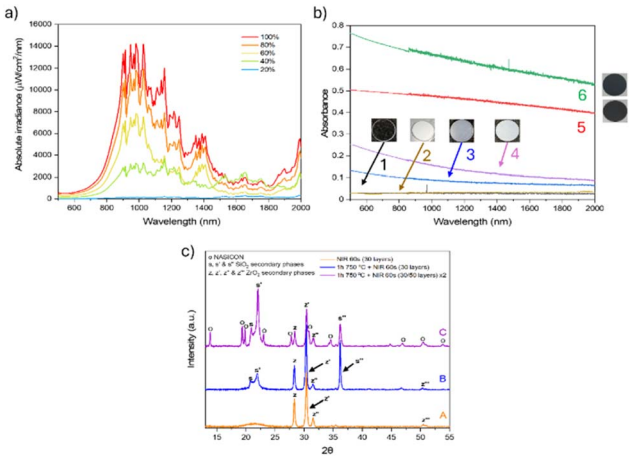

Fig. 2 (a) Output emission of NIR lamps (obtained from ref. 30, more information in the ESI†). (b) NIR absorption of (1) substrate; (2) 30 sol layers; (3) 30 sol layers, 1 h of thermal treatment at 750 °C and NIR sintering at 90% power for 60 s; (4) 50 sol layers onto 2, 1 h of thermal treatment at 750 °C and NIR sintering at 100% power for 60 s; (5): 30 sol layers and 1 h of thermal treatment at 750 °C; (6) 50 sol layers onto 2, 1 h of thermal treatment at 750 °C. (c) XRD of NIR sintered samples: (A) 30 sol layers directly sintered at 90% power for 60 s; (B) 30 sol layers, treated at 750 °C for 1 h and sintered at 90% power for 60 s; (C) 50 sol layers onto B, treated at 750 °C for 1 h and sintered at 100% power for 60 s.

heats up the film under NIR radiation. However, after a 750 °C thermal pre-treatment and a NIR sintering step for 60 seconds (heating step at 90% power), the NASICON phase was still not observed (diffractogram B, Fig. 2c).

After NIR treatment, the black coloration disappears (number 3, Fig. 2b) suggesting that a combustion reaction between carbon and O_2 happened. DSC/TGA analysis (Fig. 1b) showed that this combustion takes place at temperatures above 950 °C. Furthermore, SiO_2 phases appear in the XRD after this treatment with peaks at 20.90°, 22.1° and 36.1° (s, s′ and s″ in diffractogram B, Fig. 2c). The s′ peak (tetragonal silica) is observed starting at 800 °C (thermal stage XRD, ESI, Fig. S1a†) but the other 2 peaks are not seen until reaching 950 °C (ESI, Fig. S1b†). However, a similar peak intensity for s and s″ is only obtained when sintering at 1000 °C after 15 min (ESI, Fig. S1c and d†). This confirms that a temperature of ≥1000 °C was reached. Hence, we attribute the non-formation of NASICONs to (1) a short sintering time (NASICON phase was observed after 30 min of sintering at 1000 °C in Fig. S1d†), (2) a too thin film (and, consequently, an insufficient absorption of NIR radiation) and (3) insufficient temperature (*i.e.*, we anticipate that a higher temperature is required to obtain NASICONs in such a short time). Interestingly, after depositing a thicker film on top of the aforementioned film (50 more layers, 80 layers in total) and heating it again for 1 h at 750 °C, a higher NIR absorbance is obtained (number 6, Fig. 2b). Furthermore, after a new NIR sintering process (60 s heating step at 100% power), the formation of NASICONs occurs (diffractogram C, Fig. 2c). We ascribe increasing the thickness to improving the film's ability to absorb NIR radiation and also introducing more carbon (which led to more energy generated *in situ* during the combustion reaction). This combination of factors enabled the formation of NASICONs in a significantly shorter time, *i.e.*, the production time is reduced from 3 h to 60 s. A video of this process is given in Fig. S2.†

The NIR-sintered sample was compared with an oven-sintered sample (1000 °C for 3 h). A morphology/surface comparison between both samples is shown in Fig. 3. In the oven-processed films, the NASICON phase forms into islands connected by SiO_2 (identified by EDS, Fig. 3a–c). The NIR-sintered NASICON film is much more uniform at the micron level (Fig. 3e and f) with these two phases not being clearly differentiated. The longer thermal treatment of the oven sample facilitates the massive growth of the silica phase (Fig. 4a) generating this heterogeneous surface. At the submicron scale (Fig. 3c) secondary phases are evident within the oven sintered NASICON film, compared to the NIR sintered microstructure (Fig. 3g) where there appear to be two phases but with a much smaller particle size than the oven sintered microstructure. The lower intensity of NASICON peaks in XRD analysis (Fig. 4) is attributed to shorter sintering times, but at least 30 min of thermal treatment in the oven are needed to start forming NASICONs (Fig. S1†), confirming that NIR heating allows much faster processing.[29,30,36]

Whilst the NIR processed films have a much finer microstructure than the oven processed films, the ionic conductivity at similar thickness (around 10 microns, Fig. 3d and h) is equally low. Impedance measurements (method details in ESI,

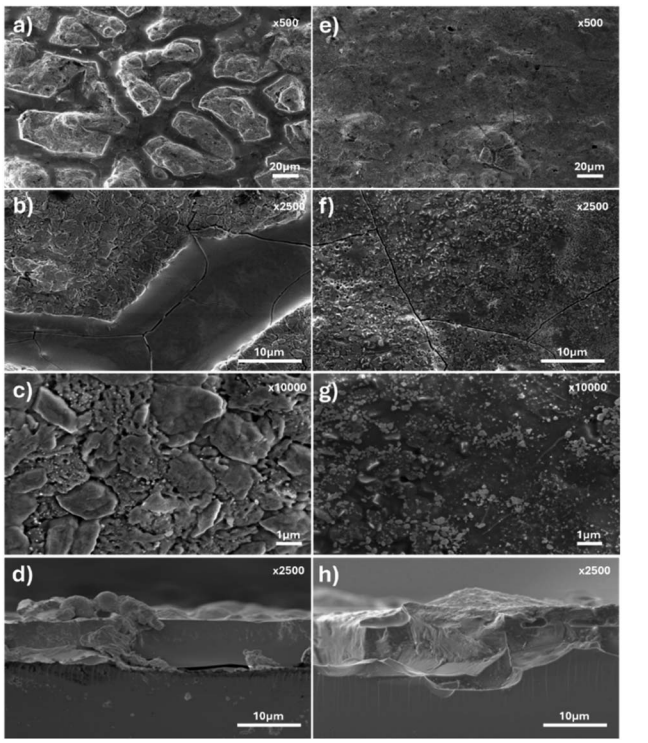

Fig. 3 SEM images from (a–d) oven sintered (1000 °C) sprayed NASICON and (e–h) NIR sintered sprayed NASICON films. (d and h) Cross sections (oven and NIR, respectively).

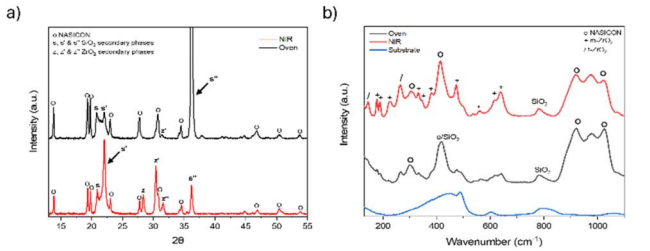

Fig. 4 (a) XRD of sol films sintered in a conventional oven and NIR oven. (b) Raman spectra of the fused silica substrate, NIR-sintered film and oven-sintered film.

Fig. S3†) show that both techniques result in an ionic conductivity of $\sim 1 \times 10^{-6}$ S cm^{-1}. These low values could be related to the high presence of detrimental zirconium oxide phases in the NIR sintered film[41] detected by XRD and Raman analysis (Fig. 4a and b, respectively). The presence of monoclinic ZrO_2 can be related to a sintering temperature $\geq$1000 °C.[20] Further optimization of the NIR treatment (*e.g.*, reducing the process time) could avoid the formation of this phase while maintaining the formation of NASICONs. Raman analysis shows a lower presence of the ZrO_2 (monoclinic and tetragonal) for the oven sample (Fig. 4b), however, its heterogeneous microstructure doesn't allow higher ionic conductivity values to be reached.

Conclusions

In conclusion, we present the first report of NASICONs sintered by NIR. We demonstrated a new method to obtain $Na_3Zr_2Si_2PO_{12}$ films by combining this heating technology and the deposition of a water-based sol precursor by spray coating. The absorption of NIR radiation was enhanced with a black carbon residue allowing crystallisation of the NASICON phase. The production time of the NASICON films was reduced and a more homogeneous surface was obtained than oven-treated films. Further work is needed to reduce secondary phases and increase ionic conductivity.

We believe that this innovative approach can be used to sinter a wide range of ceramic coatings with the potential for faster sintering times, reducing interlayer diffusion and increasing the range of potential substrates.

Data availability

The data supporting this article have been included as part of the ESI.†

Author contributions

RMV: experimental, methodology, investigation, formal analysis, write up, conceptualisation, data curation, writing original draft, review and editing; RG: experimental, data curation, write up, conceptualisation, investigation, review and editing; AS: write up; CD-D: experimental, review and editing; TD: experimental, formal analysis, review and editing; SR: experimental, review and editing; PJH: supervision, resources, review and editing; JB: conceptualisation, methodology, funding, supervision, experimental, resources, writing original draft, review and editing.

Conflicts of interest

There are no conflicts to declare.

Acknowledgements

We gratefully acknowledge funding from the EPSRC ECR Fellowship NoRESt EP/S03711X/1 (JB, RMV, AS, BG,and CD-D), EPSRC/Tata Steel for co-sponsoring an iCASE PhD studentship (Grant number: 2610332) (Voucher # 20000176) for SR and the Sustain Hub (EP/S018107/1) for PJH and HEFCW for the funding capital grant for the STA. The authors would like to acknowledge the access to characterisation equipment at the Swansea University Advanced Imaging of Materials (AIM) facility, which was funded in part by the EPSRC (EP/M028267/1) and the European Regional Development Fund through the Welsh Government (80708).

Notes and references

1 Y. Miyachi, G. Sakai, K. Shimanoe and N. Yamazoe, *Sens. Actuators, B*, 2003, **93**, 250–256.
2 X. Liang, B. Wang, H. Zhang, Q. Diao, B. Quan and G. Lu, *Sens. Actuators, B*, 2013, **187**, 522–532.
3 S. Balagopal, T. Landro, S. Zecevic, D. Sutija, S. Elangovan and A. Khandkar, *Sep. Purif. Technol.*, 1999, **15**, 231–237.
4 N. Kim, S. Jeong, W. Go and Y. Kim, *Water Res.*, 2022, **215**, 118250.
5 M. Sozak, T. Nazarenus, J. Exner, J. Kita and R. Moos, *J. Mater. Sci.*, 2023, **58**, 10108–10119.
6 A. Chakraborty, R. Thirupathi, S. Bhattacharyya, K. Singh and S. Omar, *J. Power Sources*, 2023, **572**, 233092.
7 R. Thirupathi, V. Kumari, S. Chakrabarty and S. Omar, *Prog. Mater. Sci.*, 2023, **137**, 101128.
8 N. Anantharamulu, K. Koteswara Rao, G. Rambabu, B. Vijaya Kumar, V. Radha and M. Vithal, *J. Mater. Sci.*, 2011, **46**, 2821–2837.
9 C. Wen, Z. Luo, X. Liu, Y. Wu, J. Tong, H. Liang, Q. Zhang, T. Ning and A. Lu, *Solid State Ionics*, 2023, **393**, 116185.
10 S. Naqash, Q. Ma, F. Tietz and O. Guillon, *Solid State Ionics*, 2017, **302**, 83–91.
11 R. Hill, A. Peretti, L. J. Small, E. D. Spoerke and Y.-T. Cheng, *ACS Appl. Energy Mater.*, 2023, **6**, 2515–2523.
12 A. Jalalian-Khakshour, C. O. Phillips, L. Jackson, T. O. Dunlop, S. Margadonna and D. Deganello, *J. Mater. Sci.*, 2020, **55**, 2291–2302.
13 M. Niazmand, Z. Khakpour and A. Mortazavi, *J. Alloys Compd.*, 2019, **798**, 311–319.
14 Z. Yao, K. Zhu, J. Zhang, X. Li, J. Chen, J. Wang, K. Yan and J. Liu, *J. Mater. Sci.: Mater. Electron.*, 2021, **32**, 24834–24844.

15 L. Huang, Z. Wen, M. Wu, X. Wu, Y. Liu and X. Wang, *J. Power Sources*, 2011, **196**, 6943–6946.
16 A. Ahmad, C. Glasgow and T. A. Wheat, *Solid State Ionics*, 1995, **76**, 143–154.
17 Y. Shimizu, S. Michishita and T. Murata, *Jpn. J. Appl. Phys.*, 1995, **34**, L833–L836.
18 Y. Shimizu and T. Ushijima, *Solid State Ionics*, 2000, **132**, 143–148.
19 S. Zhang, B. Quan, Z. Zhao, B. Zhao, Y. He and W. Chen, *Mater. Lett.*, 2004, **58**, 226–229.
20 N. S. Bell, C. Edney, J. S. Wheeler, D. Ingersoll and E. D. Spoerke, *J. Am. Ceram. Soc.*, 2014, **97**, 3744–3748.
21 J. A. S. Oh, X. Xu, Z. Zeng, K. Wang, N. Y. J. Tan, E. Kok, J. Huang and L. Lu, *Energy Environ. Mater.*, 2023, **6**, e12472.
22 M. Zhou and A. Ahmad, *Sens. Actuators, B*, 2007, **122**, 419–426.
23 A. Paulus, S. Kammler, S. Heuer, M. C. Paulus, P. Jakes, J. Granwehr and R.-A. Eichel, *J. Electrochem. Soc.*, 2019, **166**, A5403.
24 J. Exner, T. Nazarenus, D. Hanft, J. Kita and R. Moos, *Adv. Mater.*, 2020, **32**, 1908104.
25 P. Jiang, G. Du, Y. Shi, F. She, P. Guo, G. Qian, X. Lu, F. Xie and X. Lu, *Chem. Eng. J.*, 2023, **451**, 138771.
26 J.-S. Lee, C.-M. Chang, Y. I. L. Lee, J.-H. Lee and S.-H. Hong, *J. Am. Ceram. Soc.*, 2004, **87**, 305–307.
27 X. Wang, Z. Liu, Y. Tang, J. Chen, D. Wang and Z. Mao, *J. Power Sources*, 2021, **481**, 228924.
28 D. A. Brennan, *NIR Curing of High Performance Coatings*, Swansea University, 2018.
29 J. Troughton, C. Charbonneau, M. J. Carnie, M. L. Davies, D. A. Worsley and T. M. Watson, *J. Mater. Chem. A*, 2015, **3**, 9123–9127.
30 K. Hooper, *Rapid Processing of Dye-sensitised Solar Cells using Near Infrared Radiative Heating*, Swansea university, 2014.
31 W. Gu, W. Yuan, T. Zhong, X. Wu, C. Zhou, J. Lin and Z. Cui, *RSC Adv.*, 2018, **8**, 30215–30222.
32 H.-J. Hwang, K.-H. Oh and H.-S. Kim, *Sci. Rep.*, 2016, **6**, 19696.
33 T. Watson, I. Mabbett and D. Worsley, *MRS Online Proc. Libr.*, 2010, **1211**, 806.
34 P.-H. Lee, B.-T. Li, C.-F. Lee, Z.-H. Huang, Y.-C. Huang and W.-F. Su, *Sol. Energy Mater. Sol. Cells*, 2020, **208**, 110352.
35 M.-H. Jao, C.-C. Cheng, C.-F. Lu, K.-C. Hsiao and W.-F. Su, *J. Mater. Chem. C*, 2018, **6**, 9941–9949.
36 K. Hooper, M. Carnie, C. Charbonneau and T. Watson, *Int. J. Photoenergy*, 2014, 953623.
37 J. Baker, K. Hooper, S. Meroni, A. Pockett, J. McGettrick, Z. Wei, R. Escalante, G. Oskam, M. Carnie and T. Watson, *J. Mater. Chem. A*, 2017, **5**, 18643–18650.
38 A. Tiliakos, M. Iordache and A. Marinoiu, *Appl. Sci.*, 2021, **11**(18), 8432.
39 J. Amaro-Gahete, D. Esquivel, J. R. Ruiz, C. Jiménez-Sanchidrián and F. J. Romero-Salguero, *Appl. Catal., A*, 2019, **585**, 117190.
40 F. De Rossi, J. A. Baker, D. Beynon, K. E. A. Hooper, S. M. P. Meroni, D. Williams, Z. Wei, A. Yasin, C. Charbonneau, E. H. Jewell and T. M. Watson, *Adv. Mater. Technol.*, 2018, **3**, 2–6.
41 M. Samiee, B. Radhakrishnan, Z. Rice, Z. Deng, Y. S. Meng, S. P. Ong and J. Luo, *J. Power Sources*, 2017, **347**, 229–237.